Induced transparency in nanoscale plasmonic resonator systems

Hua Lu, Xueming Liu,* Dong Mao, Yongkang Gong, and Guoxi Wang

State Key Laboratory of Transient Optics and Photonics, Xi'an Institute of Optics and Precision Mechanics, Chinese Academy of Sciences, Xi'an 710119, China

**Corresponding author: liuxueming72@yahoo.com*

Received May 31, 2011; revised July 15, 2011; accepted July 20, 2011; posted July 21, 2011 (Doc. ID 148400); published August 15, 2011

An optical effect analogous to electromagnetically induced transparency (EIT) is observed in nanoscale plasmonic resonator systems. The system consists of a slot cavity as well as plasmonic bus and resonant waveguides, where the phase-matching condition of the resonant waveguide is tunable for the generation of an obvious EIT-like coupled resonator-induced transparency effect. A dynamic theory is utilized to exactly analyze the influence of physical parameters on transmission characteristics. The transparency effect induced by coupled resonance may have potential applications for nanoscale optical switching, nanolaser, and slow-light devices in highly integrated optical circuits. © 2011 Optical Society of America

OCIS codes: 240.6680, 310.6628, 230.4555, 130.2790, 130.3120.

Electromagnetically induced transparency (EIT) occurs in atomic systems as a result of quantum interference induced by coherently driving the atom with an external laser [1,2]. Recent theoretical analyses have revealed that a novel phenomenon analogous to EIT in atomic systems can occur in photonic resonator systems due to coherent interference of coupled optical resonators, which is known as coupled resonator-induced transparency (CRIT) [3,4]. Moreover, experimental demonstrations of CRIT have been reported in various resonator systems such as coherently coupled Fabry–Perot (F–P) resonators [5], coupled microring resonators, [6], and coupled whispering-gallery microresonators [7], with observations of slow-light effect [8]. Nowadays, the use of novel techniques to fabricate small structures to control light has been exciting developments in optical physics [2]. Electromagnetic waves trapped on metal–dielectric interfaces and coupled to propagating free electron oscillations in the metals, known as surface plasmon polaritons (SPPs), are regarded as the most promising way for realization of highly integrated optical circuits due to significant overcoming of classical diffraction and manipulation of light in a nanoscale domain [9–11]. A large number of devices based on SPPs, such as all-optical switches [12,13], modulators [14], polarization analyzers [15], optical amplifiers [16], and Bragg reflectors [17,18], have been demonstrated experimentally and simulated numerically. Among these plasmonic devices, metal–dielectric–metal (MIM) waveguides have the deep subwavelength confinement of light with an acceptable length for SPP propagation. These unique features of MIM waveguides can be utilized to realize truly nanoscale photonic functionality and circuitry [11]. Recent research illustrates that optical resonators in nanoscale MIM plasmonic structures possess some similar properties to the resonators in microscale dielectric waveguide and photonic crystal systems [19–22]. Moreover, plasmon-induced transparency was found in the metamaterial due to a Fano resonance analogous to the EIT effect [23]. These results may open up a pathway in photonics and offer prospects of smaller devices for the manipulation and transmission of light.

In this Letter, we investigate numerically the EIT-like CRIT effect in the nanoscale plasmonic resonator system, which consists of a slot cavity in the middle of the bus and resonant waveguides. This system is different from the configuration reported by Han *et al.* [22]. The finite-difference time-domain (FDTD) results demonstrate that the transparency resonance peak can be tuned by adjusting the length and refractive index of the resonant waveguide. In addition, the influence of the coupling distance between the slot cavity and resonant waveguide on transmission characteristics can be accurately analyzed by the temporal coupled mode theory.

Figure 1 shows the nanoscale plasmonic resonator system. When a TM-polarized plane wave is injected into the MIM structure, the incident light will be coupled into the bus waveguide and SPP waves are formed on the two metal interfaces and confined in the central layer. The metallic claddings are assumed as silver, whose frequency-dependent complex permittivity can be described by the well-known Drude model, $\varepsilon_m(\omega) = \varepsilon_\infty - \omega_p^2/[\omega(\omega + i\gamma)]$. Here, ε_∞ is the dielectric constant at the infinite frequency and γ and ω_p stand for the electron collision and bulk plasma frequencies, respectively. ω is the angular frequency of incident light in a vacuum. These parameters for silver can be set as $\varepsilon_\infty = 3.7$, $\omega_p = 9.1\,\text{eV}$, and $\gamma = 0.018\,\text{eV}$ [17]. The MIM plasmonic structure possesses mirror symmetry with respect to the reference plane. The length and width of the resonant

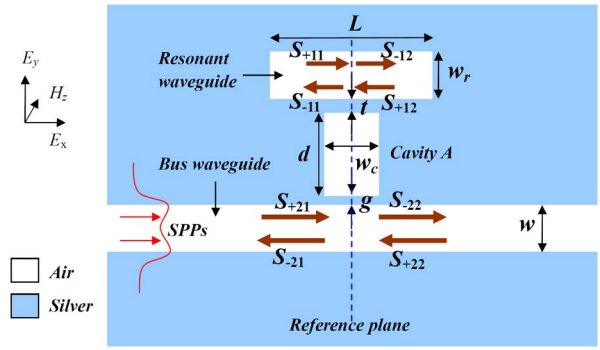

Fig. 1. (Color online) Schematic diagram of the nanoscale plasmonic resonator system.

waveguide (cavity A) are L and w_r (d and w_c), respectively. Here, the transmission characteristics of the nanoscale resonator system can be analyzed by the temporal coupled mode theory [24,25]. To simplify the theoretical model, the coupling loss between cavity A and the waveguides and the propagation loss in the bus waveguide are not considered. As shown in Fig. 1, the amplitudes of the incoming and outgoing waves into cavity A are denoted by S_{+ij} and S_{-ij} $(i,j = 1, 2)$. S is normalized such that $|S|^2$ represents the power of the wave. When an optical wave with frequency ω is launched only from the input port of the bus waveguide ($S_{+22} = 0$), the time evolution of the normalized amplitude a of cavity A can be expressed as

$$\frac{da}{dt} = \left(j\omega_0 - \frac{\omega_0}{Q_i} - \frac{\omega_0}{2Q_1} - \frac{\omega_0}{2Q_2}\right)a + S_{+21}e^{j\theta_0}\sqrt{\frac{\omega_0}{2Q_2}} + S_{+11}e^{j\theta_1}\sqrt{\frac{\omega_0}{2Q_1}} + S_{+12}e^{j\theta_2}\sqrt{\frac{\omega_0}{2Q_1}}. \quad (1)$$

Here, ω_0 is the resonant frequency of the cavity. Q_i is the quality factor due to the intrinsic loss in the cavity and Q_1 and Q_2 are the quality factors related to the decay rate into the resonant and bus waveguides, respectively. θ_0 (θ_1 and θ_2) is the phase of the coupling coefficient between cavity A and the bus (resonant) waveguide. The relationships between the amplitude of cavity A and the incoming/outgoing waves in the waveguides are derived as

$$S_{-22} = S_{+21} - e^{-j\theta_0}\sqrt{\frac{\omega_0}{2Q_2}}a, \quad (2)$$

$$S_{-11} = S_{+12} - e^{-j\theta_1}\sqrt{\frac{\omega_0}{2Q_1}}a, \quad (3)$$

$$S_{-12} = S_{+11} - e^{-j\theta_2}\sqrt{\frac{\omega_0}{2Q_1}}a. \quad (4)$$

The waves in the resonant waveguide should satisfy a steady-state relation: $S_{+11} = S_{-11}\sigma e^{-j\varphi}$ and $S_{+12} = S_{-12}\sigma e^{-j\varphi}$ $(0 < \sigma < 1)$. Here, φ and σ are the phase shift and attenuation terms of the SPP mode during a round trip in the right (or left) waveguide of the reference plane, respectively. When $\theta_1 = \theta_2$, the transmission T of the output port is expressed as

$$T = \left|\frac{S_{-22}}{S_{+21}}\right|^2 = \left|\frac{j\left(\frac{\omega}{\omega_0} - 1\right) + \frac{1}{Q_i} - \frac{1}{2Q_1} + \frac{1}{Q_1}\frac{1}{1-\delta e^{-j\varphi}}}{j\left(\frac{\omega}{\omega_0} - 1\right) + \frac{1}{Q_i} - \frac{1}{2Q_1} + \frac{1}{2Q_2} + \frac{1}{Q_1}\frac{1}{1-\delta e^{-j\varphi}}}\right|^2. \quad (5)$$

From the above equation, we note that the transmission relies on the phase term φ, which can be described as

$$\varphi(\omega) = \frac{\omega \mathrm{Re}(n_{\mathrm{eff}})L}{c} + \theta, \quad (6)$$

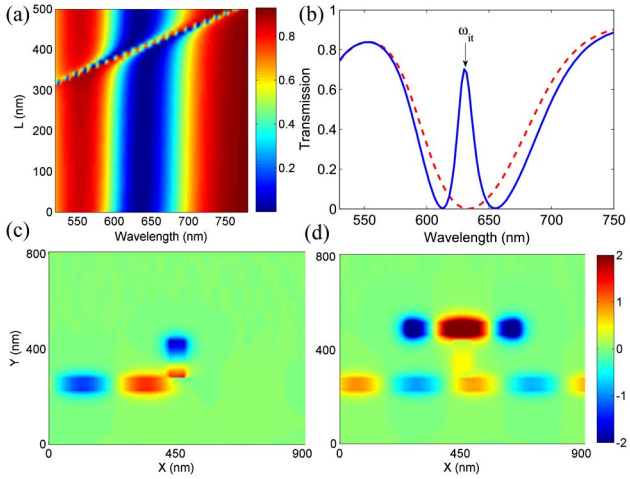

Fig. 2. (Color online) (a) Evolution of transmission spectrum with the length L of resonant waveguide in the resonator system with $d = 150$ nm, $g = 5$ nm, and $t = 30$ nm. (b) Transmission spectra without (red dashed curve) and with (blue solid curve) resonant waveguide when $L = 400$ nm. (c) and (d) Field distributions of H_z at the transmitted dip wavelength with $L = 0$ nm and induced transparency wavelength with $L = 400$ nm (Media 1).

where θ represents the reflective phase shift on a metal facet of the resonant waveguide. n_{eff} stands for the effective refractive index of the SPP mode in cavity A, which can achieved by the dispersion equations [19,26]. From Eq. (6), we find that the phase φ also relies on L. The FDTD method is utilized to investigate the dependence of transmission characteristics on L [21,27]. The geometric parameters are set as $d = 150$ nm, $g = 5$ nm, $t = 30$ nm, and $w_r = w_c = w = 50$ nm. Figure 2(a) shows the evolution of the transmission spectrum with L. It is found that a high transparency spectrum line appears in the transmitted dip when L reaches special values. The transmission spectra with $L = 0$ and 400 nm are depicted in Fig. 2(b). We find that the spectrum exhibits a narrow transparency peak in the center of a broader transmitted dip. This is the EIT-like transmission spectrum, which is different from the results in Ref. [21]. Figures 2(c) and 2(d) shows the field distributions of H_z at the transmitted dip wavelength of 634 nm with $L = 0$ nm and transparency-peak wavelength of 630 nm with $L = 400$ nm, respectively. The results are in good agreement with the transmission spectra in Fig. 2(b). It is worth noting that the optical wave coupled into the resonant waveguide exhibits F–P oscillation and forms a standing wave mode when φ approximately satisfies the phase-matching condition: $\varphi(\omega) = 2\pi$. The coupled resonance induces transparency effect in the bus waveguide [25].

From Eq. (5), the factor quality Q_1 controlled by the coupling distance t between cavity A and the resonant waveguide can affect the transmission properties. Figure 3(a) shows transmission spectra at different coupling distances t. It is found that the induced transparency wavelength is nearly invariable due to the scarcely unchanged phase-matching condition, while the transparency peak exhibits a decrease, which is consistent with the theoretical result, as shown in Fig. 3(b). The dependence of transmission spectrum on the resonance wavelength determined by the length d of cavity A is

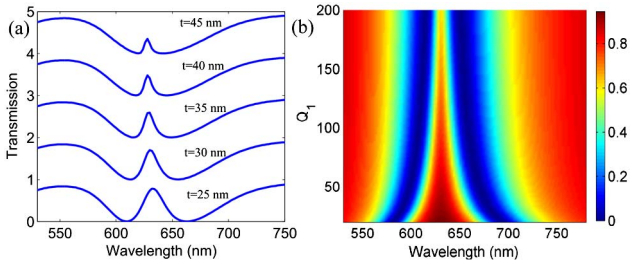

Fig. 3. (Color online) (a) Transmission spectra at different coupling distances t with $g = 5\,\text{nm}$, $L = 400\,\text{nm}$, $d = 150\,\text{nm}$, and $w = w_r = w_c = 50\,\text{nm}$. (b) Evolution of transmission spectrum with Q_1. The results are calculated by a theoretical model with assumed parameters $Q_i = 220$, $Q_2 = 7$, $\theta = 0.6$, $L = 400\,\text{nm}$, $\omega_0 = 2.973 \times 10^{15}\,\text{rad/s}$, and $\sigma = 0.98$.

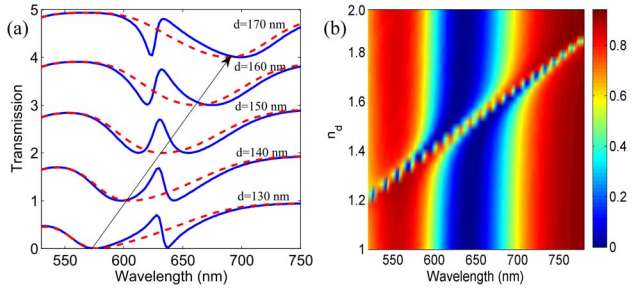

Fig. 4. (Color online) (a) Transmission spectra at different lengths d in the plasmonic structures with $L = 0\,\text{nm}$ (red dashed line) and $L = 400\,\text{nm}$ (blue solid line). (b) Evolution of transmission spectrum with the refractive index n_d of the resonant waveguide. The other parameters are set as $d = 150\,\text{nm}$, $g = 5\,\text{nm}$, $t = 30\,\text{nm}$, and $L = 250\,\text{nm}$.

investigated by FDTD simulations and shown in Fig. 4(a). We find that the resonance wavelength of the cavity possesses a linear redshift, which is in accordance with the results in Ref. [19]. Since the phase-matching condition is nearly unchanged, the transparency peak has no obvious shift. Meanwhile, the transparency spectrum is obvious when the misalignment between the resonance wavelengths of cavity A and the resonant waveguide is slight. Thus, the transparency spectrum line can be effectively modulated by altering the lengths of cavity A and the resonant waveguide. From Eq. (6), the transparency resonance is influenced by the effective refractive index n_{eff} of the resonant waveguide. According to the dispersion equation [19], n_{eff} relies on the refractive index n_d in the waveguide. Figure 4(b) shows the influence of n_d on the transmission spectrum. It is found that the transparency resonance wavelength possesses a redshift with the increase of n_d. The nanoscale optical switching may be realized in this resonator system by filling the resonant waveguide with Kerr nonlinear material due to the strong resonant effect and narrow induced transparency bandwidth, as shown in Figs. 2(d) and 2(b).

In summary, the EIT-like CRIT effect has been investigated numerically in the nanoscale plasmonic resonator system which consists of a slot cavity in the middle of the bus and resonant waveguides. The induced transparency peak can be manipulated by adjusting the phase-matching condition (controlled by the length and refractive index) of the resonant waveguide. The transmission characteristics also depend on the coupling distance between the slot cavity and the resonant waveguide. The FDTD results can be accurately analyzed by the theoretical model. The optical transparency effect induced by the coupled resonance may be applied for nanoscale optical switching, nanolaser, and slow-light devices in highly integrated optical circuits.

This work was supported by the National Natural Science Foundation of China (NSFC) under grants 10874239 and 10604066.

References

1. M. Fleischhauer, A. Imamoglu, and J. P. Marangos, Rev. Mod. Phys. **77**, 633 (2005).
2. R. W. Boyd and D. J. Gauthier, Nature **441**, 701 (2006).
3. D. D. Smith, H. Chang, K. A. Fuller, A. T. Rosenberger, and R. W. Boyd, Phys. Rev. A **69**, 063804 (2004).
4. Y. Zhang, S. Darmawan, L. Tobing, T. Mei, and D. Zhang, J. Opt. Soc. Am. B **28**, 28 (2011).
5. X. Yang, M. Yu, D. Kwong, and C. Wong, Phys. Rev. Lett. **102**, 173902 (2009).
6. Q. Xu, S. Sandhu, M. Povinelli, J. Shakya, S. Fan, and M. Lipson, Phys. Rev. Lett. **96**, 123901 (2006).
7. A. Naweed, G. Farca, S. I. Shopova, and A. T. Rosenberger, Phys. Rev. A **71**, 043804 (2005).
8. K. Totsuka, N. Kobayashi, and M. Tomita, Phys. Rev. Lett. **98**, 213904 (2007).
9. W. Barnes, A. Dereux, and T. Ebbesen, Nature **424**, 824 (2003).
10. S. I. Bozhevolnyi, V. S. Volkov, E. Devaux, J. Y. Laluet, and T. W. Ebbesen, Nature **440**, 508 (2006).
11. R. Zia, J. A. Schuller, A. Chandran, and M. L. Brongersma, Mater. Today **9**, 20 (2006).
12. G. A. Wurtz, R. Pollard, and A. V. Zayats, Phys. Rev. Lett. **97**, 057402 (2006).
13. H. Lu, X. Liu, L. Wang, Y. Gong, and D. Mao, Opt. Express **19**, 2910 (2011).
14. T. Nikolajsen, K. Leosson, and S. I. Bozhevolnyi, Appl. Phys. Lett. **85**, 5833 (2004).
15. S. Yang, W. Chen, R. Nelson, and Q. Zhan, Opt. Lett. **34**, 3047 (2009).
16. I. D. Leon and P. Berini, Nat. Photonics **4**, 382 (2010).
17. J. Park, H. Kim, and B. Lee, Opt. Express **16**, 413 (2008).
18. A. Boltasseva, S. Bozhevolnyi, T. Nikolajsen, and K. Leosson, J. Lightwave Technol. **24**, 912 (2006).
19. F. Hu, H. Yi, and Z. Zhou, Opt. Lett. **36**, 1500 (2011).
20. A. Hosseini and Y. Massoud, Appl. Phys. Lett. **90**, 181102 (2007).
21. H. Lu, X. Liu, D. Mao, L. Wang, and Y. Gong, Opt. Express **18**, 17922 (2010).
22. Z. Han and S. Bozhevolnyi, Opt. Express **19**, 3251 (2011).
23. B. Luk'yanchuk, N. Zheludev, S. Maier, N. Halas, P. Nordlander, H. Giessen, and C. Chong, Nat. Mater. **9**, 707 (2010).
24. H. A. Haus, *Waves and Fields in Optoelectronics* (Prentice-Hall, 1984), Chap. 7.
25. J. Zhou, D. Mu, J. Yang, W. Han, and X. Di, Opt. Express **19**, 4856 (2011).
26. X. S. Lin and X. G. Huang, Opt. Lett. **33**, 2874 (2008).
27. A. Taflove and S. Hagness, *Computational Electrodynamics: The Finite-Difference Time-Domain Method*, 2nd ed. (Artech House, 2000).